EFFECT OF RANDOM PRE-STRESSED FRICTION LOSS ON THE PERFORMANCE OF A SUSPEN-DOME STRUCTURE

Ren‐Zhang Yan [1, 2, *], Mei‐Hao Zhu [3], Ting Liu [1, 2], Jia‐Qi Liu [1, 2] and Zhi‐Hua Chen [4]

[1] *State Key Laboratory of Mountain Bridge and Tunnel Engineering, Chongqing Jiaotong University, Chongqing 400074, China*

[2] *School of Civil Engineering, Chongqing Jiaotong University, Chongqing 400074, China*

[3] *Design and Development Department, China Construction Science and Technology Co., Ltd. Sichuan Branch, Chengdu 610213, China*

[4] *School of Civil Engineering, Tianjin University, Tianjin 300072, China*

* *(Corresponding author: E-mail: rz_yan@cqjtu.edu.cn)*

A B S T R A C T

The key to the high-efficiency performance of the suspen-dome structure is to apply the pre-stressed design value to the structure accurately. However, engineering practice has found that the use of tensioning hoop cables to apply the pre-stress will produce noticeable pre-stressed friction loss (PFL), which significantly affects the safety performance of the structure. In this paper, based on a 1:10 scaled-down experiment model of a suspen-dome structure with rolling cable-strut joint installed, the random PFL (RPFL) effect of the suspen-dome on structure performance was analyzed through a probability statistics theory. First, aiming at the unequal tensioning force at both sides of the tensioned hoop cable during the tensioning process, a pre-stressed force calculation method is proposed that considers the unequal tensioning control force and RPFL at all cable–strut joints, and the reliability of this method is verified through a tension test. Then, based on the cable-joint tension test carried out in the early stage of the research group, a random mathematical model of the friction coefficient (FC) at the rolling cable–strut joint is established. And then, the cable force calculation method is used to establish the random finite element model, and independent and random changes in the FC at each rolling cable–strut joint can be considered. Subsequently, the Monte Carlo method is used to calculate the random mathematical characteristics of the mechanical performance parameters such as the member stress and joint deformation, and the obtained results are verified through a static loading experiment. In addition, to investigate the effect of random defects on structural stability, other random defects, such as the initial curvature and installation deviation, were continuously introduce based on the random finite element model. As such, we could obtain the law of the effect of multi-defect random variation coupling on the structure's ultimate bearing capacity.

1. Introduction

A new type of hybrid space structure, the suspen-dome, enhances the structural stability and ease of construction of buildings [1]. Since its proposal by Kawagucki [2], the suspen-dome has been widely used in more than 20 engineering projects [3, 4]. The high efficiency of the suspen-dome structure is achieved by accurately applying the pre-stressed design values to increase its stiffness and bearing capacity [5-7]. However, pre-stressed friction loss (PFL) is generated while tensioning the hoop cables (HCs). Zhang et al. studied the PFL of the 2008 Olympic Games Badminton Gymnasium and found, through on-site monitoring, that the total PFL of each HC was more than 35%, causing the ultimate bearing capacity of the structure to reduce by approximately 15% [8]. The PFL from the construction process of the suspen-dome structure can have a large negative effect on its performance, even threatening its safety. Zhang et al. reduced PFL by changing the type of joint and pointed out that friction results in unevenness of the internal force distribution of the structure [9]. Liu et al. analyzed the friction loss at the rolling cable–strut joint and its effect on the suspen-dome [10, 11].

Till date, studies on the analysis of the effect of PFL on the performance of the suspen-dome structure remain at the qualitative level. Therefore, the conclusions drawn by various studies vary with the analytical methods used. Existing studies use only theoretical analysis to study the PFL effect, which cannot simulate all the possible problems that could occur in the actual design and construction process[12]. Therefore, to gain a more accurate understanding of the mechanical properties of the suspen-dome structure and enable broader applications, experiments must be performed. In this study, in view of the core position of the tensegrity system in a suspen-dome and PFL in the actual construction process, the authors developed a scaled-down suspen-dome model, for which safety was accurately evaluated using specific quantitative indices, and the effect of random PFL (RPFL) on the static structure performance was explored.

2. New cable force calculation method

Several force-finding methods have been developed in the last decade. For example, Chen et al. presented an improved symmetry method that only requires the symmetry type and connectivity of the structure for analysis [13]. Zhang et al. presented an optimization approach that can easily find various equilibrium shapes [14, 15]. Liu et al. developed a double control form finding method considering the construction process for controlling both the configuration and force balance [16]. However, few methods consider the friction of the cable–strut joints [17]. When pre-stress is applied by tensioning the HCs, the actual control values at the tensioning points on both sides of the same tensioned cable may not be equal, owing to the limitations of the tensioning equipment and cable force-monitoring system. In addition, inevitable differences appear between cable–strut joints during the manufacturing process, and the friction coefficients of cable-strut joints (FCCJ) are not completely equal, increasing the complexity of the internal force distribution of the passive-tensioning cable segments. However, accurate determination of the internal force distribution of each cable segment is a prerequisite for precisely evaluating the effect by considering the effect of RPFL on the global structure performance. To simulate the pre-stressed distribution during the actual tensioning construction process, a new cable force calculation method is proposed that considers the unequal tensioning control force and different FCCJs.

2.1. Internal force calculation process of passive-tensioning cable segments

Fig. 1 shows the schematic of a continuous tensioning cable consisting of $(n-1)$ cable–strut joints and n cable segments. The tensioning values at tensioning points 1 and 2 are not equal, i.e., $[T1] \neq [T2]$, and the friction coefficients (FCs), μ_i, of the cable–strut joints are not equal, and μ_i represents the No. i cable–strut joints. To conduct the simulations and experiments, the following assumptions were made: (i) $[T1] \geq [T2]$. (ii) The tension is applied simultaneously on both sides of the tensioning cable; this does not cause any large changes in the positions of the cable–strut joints during the tensioning process.
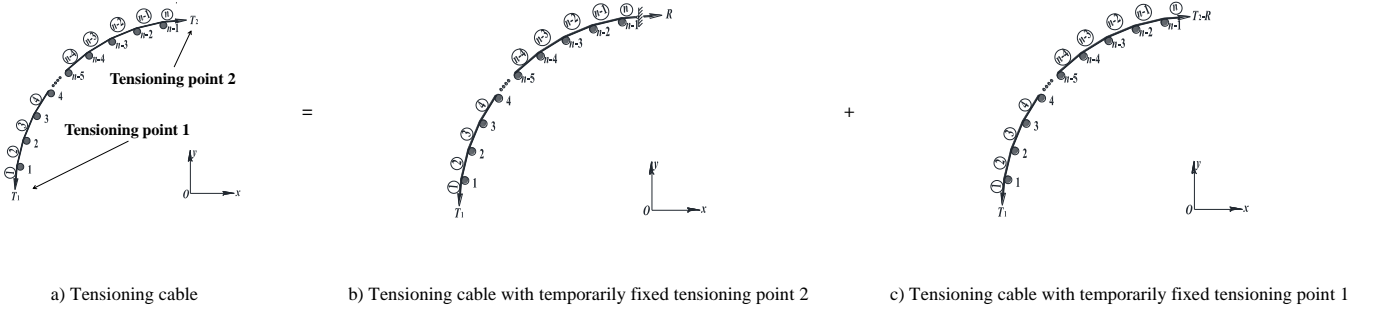
a) Tensioning cable   =   b) Tensioning cable with temporarily fixed tensioning point 2   +   c) Tensioning cable with temporarily fixed tensioning point 1

Fig. 1 Schematic of the tensioning cable

When the HC is tensioned, the cable force is gradually transferred from the tensioning points to the adjacent cable segments. The internal forces of the points and cable segments are not equal because of the friction loss that occurs at the cable–strut joints during the transfer. For generality, consider cable–strut joint i in Fig. 2 as an example. T_i is the cable force generated by the active-tensioning cable segment. Here, T_{i+1} is the cable force generated by the passive-tensioning cable segment, N_i is the vertical pressure of the cable–strut joint on the cable, and f_i is the friction force at the cable–strut joint. Assuming that the maximum static friction force at the cable–strut joint is $f_{i,max}$, and the FC is μ_i; then, according to static equilibrium and friction transfer law, the following two situations must occur:
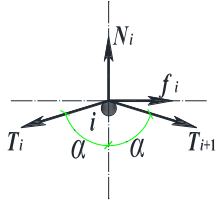
Fig. 2 Force schematic of cable–strut joint i during the tension process

① No cable sliding occurs, i.e., $T_{i+1} = 0$. This scenario is expressed as

$$\begin{cases} f_i \leq f_{i,\max} = \mu_i N_i \\ f_i = T_i \cdot \sin \alpha \\ N_i = T_i \cdot \cos \alpha \end{cases} \tag{1}$$

As indicated in Equation (1), $\tan \alpha \leq \mu_i$ and for $0° < \alpha < 90°$, $0° < \alpha < \arctan\mu_i$. That is, if $0° < \alpha < \arctan\mu_i$, the cable cannot slide, and pre-stress cannot be applied; this scenario should be avoided during the construction process.

② Cable slides, i.e., $T_{i+1} > 0$, which is expressed as

$$\begin{cases} f_i = \mu_i N_i \\ f_i + T_{i+1} \cdot \sin \alpha = T_i \cdot \sin \alpha \\ N_i = T_i \cdot \cos \alpha + T_{i+1} \cdot \cos \alpha \end{cases} \tag{2}$$

The friction force at cable–strut joint i and the internal force of cable segment $i + 1$ can be derived from Equation 2, as shown in Equations 3 and 4, respectively.

$$f_i = \mu_i T_i \frac{2\sin\alpha}{\tan\alpha + \mu_i} = k_i^1 \cdot T_i , \tag{3}$$

$$T_{i+1} = T_i \cdot \frac{\tan\alpha - \mu_i}{\tan\alpha + \mu_i} = k_i^2 \cdot T_i , \tag{4}$$

where k_i^1 is the FC and is written as $k_i^1 = \mu_i \dfrac{2\sin\alpha}{\tan\alpha + \mu_i}$.

In addition, k_i^2 is the transfer coefficient and is written as $k_i^2 = \dfrac{\tan\alpha - \mu_i}{\tan\alpha + \mu_i}$.

Here, k_i^1 and k_i^2 are only related to μ_i and α. If a tensioning cable is fixed at one end and tensioned at the other, as shown in Fig. 1b, all cable forces can be calculated in turn according to Equation 4. However, in practice, the tensioning cable is long. To reduce the effect of the friction force, both ends of the tensioning cable must be tensioned simultaneously, as shown in Fig. 1a. The transfer of cable force is bidirectional, and both ends of a tensioning cable can be the active-tensioning ends. The steps to calculate the cable internal force are as follows, which is also shown in Fig. 3.

1) Calculate α and determine μ_i, k_i^1 and k_i^2 at each cable–strut joint.

2) Temporarily fix tensioning point 2 and make the internal force of tensioning point 1 $T_1 = [T1]$. The internal force is transferred from tensioning point 1 to tensioning point 2, as shown in Fig. 1-b).

3) Calculate the internal force $T_2 \sim T_n$ from cable segment 2 to n according to Equation 4. The support reaction at the temporary fixed tensioning point 2 can be derived from the static equilibrium equation, i.e., $R = T_n$.

4) Calculate friction force $f_{n-1} \sim f_1$ from joints $n-1$ to 1 in the reverse order by using Equation 3.

5) Keep the internal force of each cable segment unchanged, release the fixed constraint at tensioning point 2, and temporarily fix tensioning point 1. Then, apply $[T_2]$ and R to tensioning point 2. The unbalanced tension at tensioning point 2 will be $\Delta T_n = [T2] - R$. This unbalanced tension is transferred from tensioning point 2 to tensioning point 1.

6) The unbalanced tension, $\Delta T_i = k_i^2 \cdot \Delta T_{i+1}$, of each cable segment is calculated from cable segment n-1 in reverse order by using Equation 4.

7) If $\Delta T_i > f_i$, the tension at tensioning point 2 can continue to be transferred to tensioning point 1, and the final internal force of cable segment i is $T_i + \Delta T_i$. If $\Delta T_i < f_i$, the tension at tensioning point 2 can no longer be transferred to tensioning point 1; the internal force from cable segments 1 to i is T_i, and the internal force from cable segments i+1 to n is $T_i + \Delta T_i$.
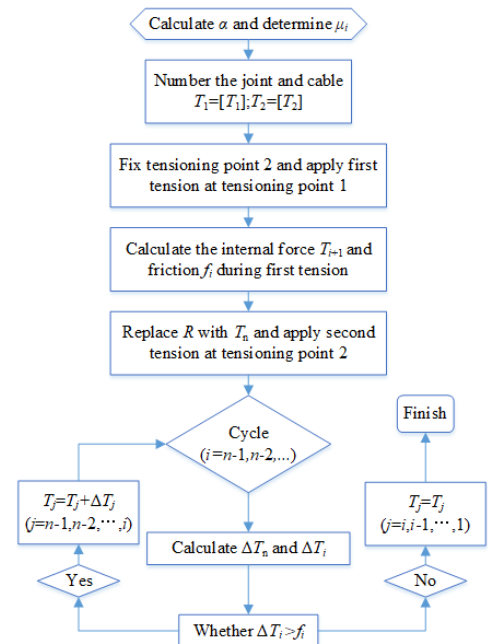

Fig. 3 Flow chart of the calculation of cable internal force

Further, if there are only two tensioning points in the HC, or the tension force in adjacent cable segments is equal to the tension segment, the internal forces of other cable segments can be directly obtained using the symmetry [18-21].

2.2. Tension test on scaled-down model

2.2.1. Experimental model

A 1:10 scaled-down suspen-dome model of the Chiping Stadium was fabricated, as shown in Fig. 4. The upper reticulated shell was assigned the Levy form, and for the lower part, a tensegrity system with seven circles of cables was used, whose HCs were numbered 1 to 7 from inside to outside. Φ12 steel wire ropes were used for the 1st and 2nd HCs, and 1×7/Φ12.7 steel strands were used for the 3rd to 7th HCs. Pre-stress was applied by tensioning the HC. One tensioning point was set at the 1st and 2nd HCs, two were symmetrically set at the 3rd HC, and four tensioning points were set at the 4th to 7th HCs. The layout diagrams of the tensioning and measurement points of the cable force are shown in Fig. 5. By combining the results of the pre-stress optimization and similarity ratio theory of the model experiment, the pre-stressed control values of HCs during the construction process were determined in Table 1. The specific tensioning equipment and control methods are detailed in [5].

a) Photograph of experimental model

Single-layer reticulated shell
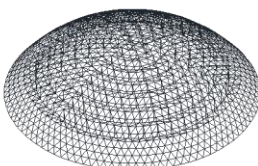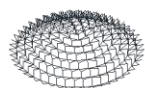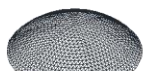
Tensegrity system

Three-dimensional graph

b) Three-dimensional graph of experimental model

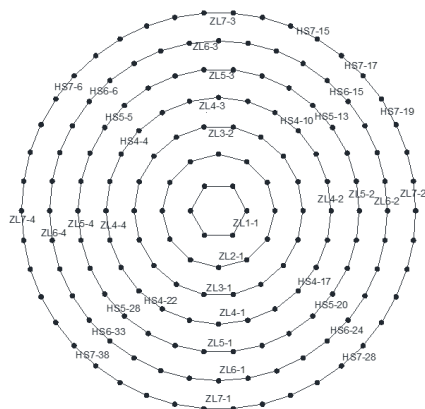**Fig. 4** Photograph and diagram of experimental model

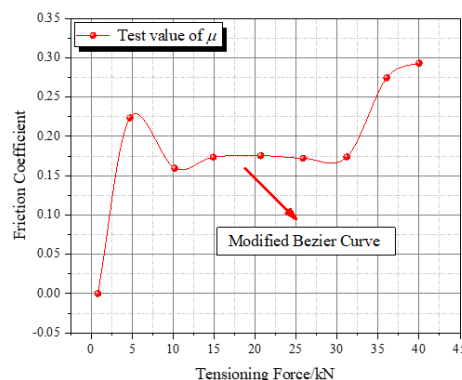**Fig. 5** Layout of tensioning points and measurement points for cable force

Fig. 6 Change curve of FC μ with the change of tension

Table 1
Pre-stressed control values

Level	1st circle	2nd circle	3rd circle	4th circle	5th circle	6th circle	7th circle
1st level (N)	100	370	495	945	1,270	2,220	4,950
2nd level (N)	300	1,770	1,600	2,000	2,470	5,040	1,1500

To reduce PFL during the tensioning process and ensure the uniform transfer of cable force, the authors independently developed a rolling cable–strut joint and used it in the model experiment. The authors had systematically studied the new joint, obtaining the changing trend of its FC fitted by the modified Bezier curve [22], as shown in Fig. 6. As indicated in Fig. 6, the FC changes with the tension force, and when the tension is small, the FC changes more drastically and presents unstable characteristics, only when the tension increases will the FC stabilize. As the FC is unstable when the internal force of the HC is small, and considering that the number of segments and joints of the outermost HC in the tension test is the largest, the internal force is the largest. Therefore, the FCs are taken as the corresponding FC when the pre-stress is 10 kN, that is, $\mu = 0.165$ when the FC has begun to stabilize. At the same time, further analysis showed that when the FC is taken as $\mu = 0.165$, this is the mean value of all the FCs measured during the cable-joint tension test. Therefore, the use of this mean value to calculate the combined effect of friction loss is considered representative.

2.2.2. Calculation results and comparative analysis

To verify the validity of the cable force calculation method for $\mu = 0.165$, the APDL of ANSYS was used to compile the internal cable force calculation program according to the calculation process shown in Fig. 3. First, the tension value at both sides of the cable is assigned according to the actual tension control value. Next, the calculated value of the internal cable force of each cable segment is calculated and compared with the actual test value. The results of the calculation, which are displayed in Fig. 7, were compared with the experimental values. The change curves of the internal cable force are shown in Fig. 8. Relative errors between the experimental and theoretical values at the measurement points are shown in Table 2.
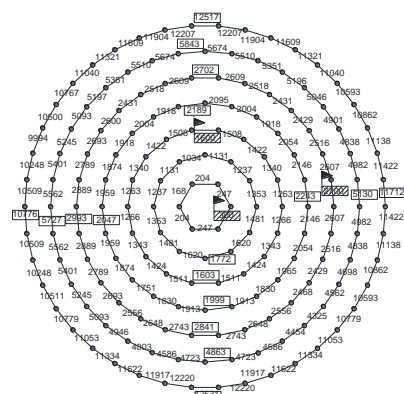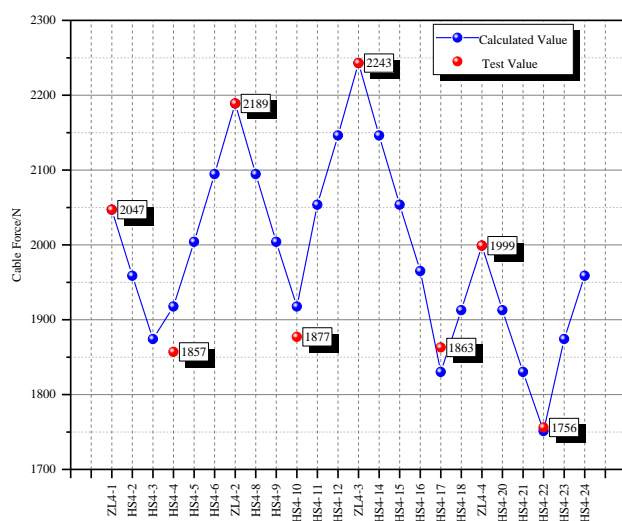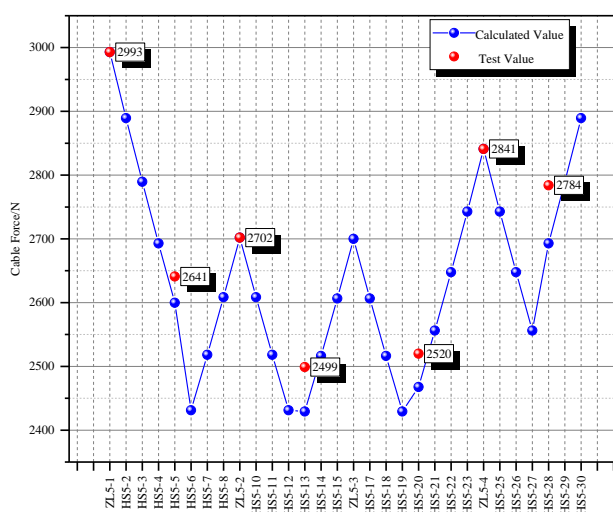

Fig. 7 Calculated values of cable force

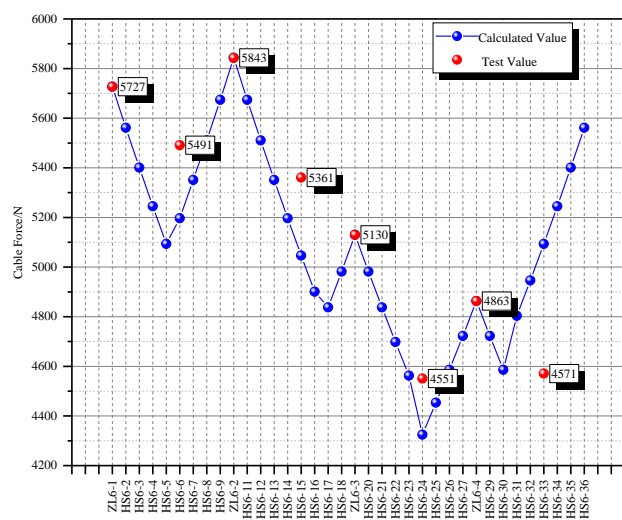Note: The value in ☐ is the actual tensioning control value at the

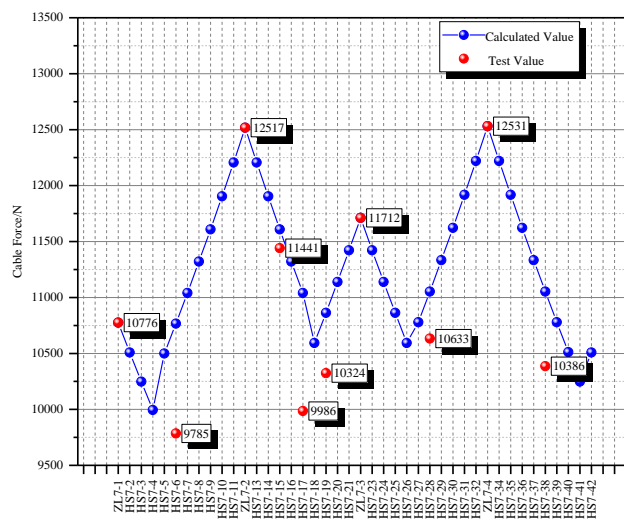tensioning point on each HC. The value in ▨ is the theoretical control

value in Table 1 which could not be monitored due to equipment fault.

a) The 4th hoop cable

b) The 5th hoop cable

c) The 6th hoop cable

d) The 7th hoop cable

Fig. 8 Change curve of internal cable force

Table 2
Relative errors in cable force calculations

Number of the measurement point	Test value/N	Calculated value/N	Relative error/%
HS4-4	1,857	1,918	-3.2%
HS4-10	1,877	1,918	-2.1%
HS4-17	1,863	1,830	1.8%
HS4-22	1,756	1,751	0.3%
HS5-5	2,641	2,600	1.6%
HS5-13	2,499	2,429	2.9%
HS5-20	2,520	2,468	2.1%
HS5-28	2,784	2693	3.4%
HS6-6	5,491	5,197	5.7%
HS6-15	5,361	5,046	6.2%
HS6-24	4,551	4,325	5.2%
HS6-33	4,671	5,093	-8.3%
HS7-6	9,785	10,767	-9.1%
HS7-15	11,441	11,609	-1.4%

HS7-17	9,986	11,040	-9.6%
HS7-19	10,324	10,862	-5.0%
HS7-28	10,633	11,053	-3.8%
HS7-38	10,386	11,053	-6.0%

As shown in Fig. 8, owing to the effect of friction, both the calculated and test values indicate that in the same tensioning cable, the cable force exhibits an approximate linear decrease while being transferred from the tensioning points to the midsection of the tensioning cable. When the tensioning cable is long, such as the 7th HC, the maximum relative error of the cable force, occurred at HS7-4, compared with the pre-stressed control value is up to 20.2%; this cannot be ignored when studying the global structure performance. As observed in Table 2, the relative errors between the test and calculated values are small, and the absolute values of them are kept within 10%. This suggests that the cable force calculation method is reliable and lays a foundation for further analysis of the effect considering the cable force errors on the global structure performance.

From the values in Table 2, the following laws are observed:

1) With the gradual increase of the pre-stressed control value from inside to outside of the HCs, the relative errors between the calculated and test values gradually increase. The absolute values of the average relative errors from the 4th to 7th HCs are 1.8, 2.5, 6.4, and 5.8%, respectively.

2) The cable force of the outermost HC is the largest. The calculated values are larger than the test values, indicating that the former underestimates the real

effect of friction. The main reason for the underestimation is that the FCCJs were taken as 0.165 uniformly throughout the theoretical calculation model. However, the FC increases with the increase in the internal cable force, as shown in Fig. 6. Therefore, for the outermost HC with the larger pre-stressed control value, using the same FC as that in the inner HC will underestimate the friction loss.

3. Random mathematical model of PFL

The FC is related to the type of contact material and the joint construction. At present, the FC is mostly determined based on actual engineering experience. The FC of the contact surface in the cable–strut joint comes down to a tribological problem. Theoretical research on this topic, however, did not start until the 15th century. Later, Amontons and Coulomb made important contributions to the field and summarized well-known classical friction laws. However, with the progress of research in tribology, it has been found that the classical law is not a general law but only suitable for special cases. New tribological theories view the FC as a comprehensive characteristic of the friction pair system, instead of an inherent characteristic of the material. It is affected by the pairing properties of material pair, static contact time, normal load, loading speed, stiffness of friction pair, sliding speed, contact geometry and physical properties of surface layer, chemical actions of environmental medium, and so on [23-26]. During the sliding process of the HC, a friction pair is formed at the cable–strut joint. In addition to being subjected to the axial tensile force, the HC

is compressed by the cable–strut joint along the normal direction. This causes the cross section shape of the HC to change continuously with the progress of the tensioning process. This, in turn, changes the FC of the friction pair. Therefore, it is difficult to obtain the exact values of FCCJ.

3.1. Value-picking study on the FC

3.1.1. FC at the traditional sliding cable–strut joint

Wang [27] and Qin et al. [28] analyzed the pre-stressed loss in the HCs of the 2008 Olympic Games Badminton Gymnasium, obtaining the value of PFL at each cable–strut joint. Liu et al. measured the FCCJ with a scaled-down suspen-dome model of the 2008 Olympic Games Badminton Gymnasium [29]. Guo et al. performed the construction monitoring service on the entire tensioning process of the Ji'nan Olympic Center Gymnasium [30]. With this, they obtained the internal forces of all HCs during the tensioning process with a magnetic flux monitor. Zhang et al. conducted experiments to study the friction generated at the cable–strut joint in a sunflower-patterned suspen-dome, and obtained PFLs of the new rolling cable–strut joints as well as the traditional sliding cable–strut joints [9]. Yuan et al. conducted an experiment on a full-scale model of the Xuzhou Olympic Center Gymnasium to derive the sliding FC at the cable–clamp joint [31]. According to the references above, the authors calculated the FCs at the traditional sliding cable–strut joints with the formula for Coulomb friction, as shown in Table 3.

Table 3
FCs at the sliding cable–strut joint in various suspen-dome constructions

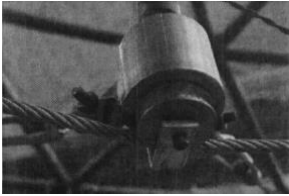| Engineering	Joint model diagram	Joint position	On-site data (average value)	Experimental value	Remarks
2008 Olympic Badminton Gymnasium [27-29]		1st circle	0.019	0.110	
		2nd circle	0.010	0.192	
		3rd circle	0.004	0.157	
		4th circle	0.024	0.115	
		5th circle	0.034	0.198	
Ji'nan Olympic Center Gymnasium [30]		Inner circle	0.012	--	
		Middle circle	0.032	--	
		Outer circle	0.036	--	
A sunflower-patterned suspen-dome [9]		1st circle	--	0.178	The roller was welded to simulate the traditional sliding cable–strut joint
		2nd circle	--	0.146	
Shandong Chiping Stadium [5][32]		Joint test	--	0.199	The roller was welded to simulate the traditional sliding cable–strut joint
Xuzhou Olympic Center Gymnasium [31]		Joint 1	--	0.123	
		Joint 2	--	0.126	
		Joint 3	--	0.129	
		Joint 4	--	0.130	
		Joint 5	--	0.130	

As indicated in Table 3, FCCJ is highly variable but follows certain laws:

1) Due to the effect of complex on-site factors, the variability of the FC observed by on-site monitoring is higher than that obtained by the experiment.

2) The FC is related to the joint position. In other words, it is related to the internal force of the HC. For example, FCCJs of the 2008 Olympic Badminton Gymnasium and Ji'nan Olympic Center Gymnasium gradually increased from the inner circle to the outer circle. This changes the cross section shape of the HC under large normal pressures.

3) The FCs obtained through the model experiments are relatively steady, varying from 0.11 to 0.20 for the same joint type.

3.1.2. FC at the new rolling cable–strut joint

Rolling friction replaces sliding friction at the rolling cable–strut joint, effectively decreasing the FCCJ. In a previous study, the research group tested the rolling cable–strut joint, which sleeve no PTFE between the pin and the roller, in the suspen-dome structure of Shandong Chiping Stadium, obtaining the values of FCCJ [5]. Fig. 7 shows the change law of the FCCJ, whose mean value is 0.165. Zhang of the Zhejiang University also measured the FC of another new rolling cable–strut joint with an experimental model [9], as shown in Table 4.

Table 4
FCs at rolling cable–strut joints

Engineering	Joint model diagram	Experimental value	
Shandong Chiping Stadium [2]		No PTFE sleeve between the pin and the roller.	0.165
		Set PTFE sleeve between the pin and the roller.	0.095
Sunflower-patterned suspen-dome [9]		0.041	

Compared with the values in Tables 3 and 4, it is easy to see the rolling cable–strut joint can effectively decrease the FC. Meanwhile, the FC can be further reduced by, for example, installing a PTFE sleeve.

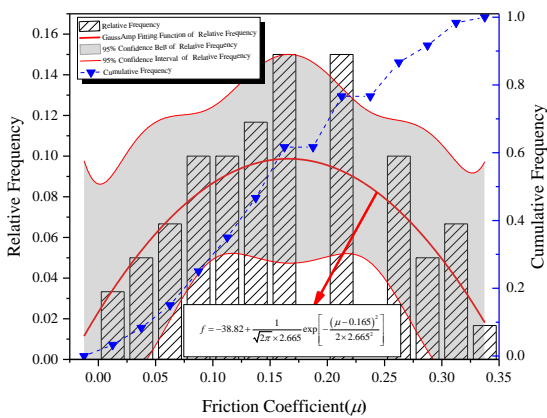### 3.2. Random mathematical model of FC at the rolling cable–strut joint

Fig. 9 Probability distribution diagram of the FC at the rolling cable–strut joint

The above analysis reveals the large discreteness of FCCJ. Different constructions have different joint structures, and therefore different FCs. However, for the same type of joint, such as the rolling cable–strut joint, the coefficient fluctuates randomly within a certain range and remains relatively uniform. In this paper, the effect of the new rolling cable–strut joint in reducing the friction loss of the suspen-dome was analyzed. Therefore, the authors further

studied previous research works and analyzed the statistical law related to the FC of the rolling cable–strut joint. A sample library of the FCCJ was created through an experiment, and a histogram of the probability distribution was drawn as shown in Fig. 9. Several factors contribute to the random fluctuation of the FC, such as the material of the contact pair, surface treatment, the angle of the adjacent cable segments, cable force, and so on. The effect of each factor in the total effect is small. Therefore, the authors assumed the FC approximately obeys the normal distribution according to the central limit theorem. In this paper, the FC μ at each cable joint is regarded as an independent random variable. As indicated in Fig. 9, the FC with no PTFE sleeve obeys the normal distribution approximately, the mean value $\bar{\mu} = 0.165$ and the mean square deviation $\sigma = 2.665$.

4. Analysis and experiment of effect of RPFL on suspen-dome structure performance

4.1. Analysis method

Since the FCCJ are random variables, the random characteristic of variables should be considered to accurately evaluate the effect of friction loss on structural performance. With the advancement of computers, numerical experiments such as the Monte Carlo method have enabled the simulation of the random characteristic of parameters, greatly promoting the development of engineering reliability. In addition, the method is a random finite element method (FEM), and there is no need to consider the complex non-linear correlations between parameters affecting the structural performance. It need only substitute the random number of each random variable into the finite element control equations repeatedly, to obtain the solution of a group of variables. Then, the distribution characteristics of the variables can be evaluated using statistical methods.

The basic idea of the Monte Carlo method is as follows: For a basic variable, i.e., the FC μ_{i_j}, at each cable–strut joint taken from 1,000 samples according to the normal distribution in the random mathematical model of Section 3. Then, the structure considering the effect of friction was calculated 1,000 times to verify the mean and the mean square deviation of each output variable. The mechanical properties of the structure were extracted as per the requirement. 1000 groups of structural-performance indices were obtained to form a sample library for the statistical analysis.
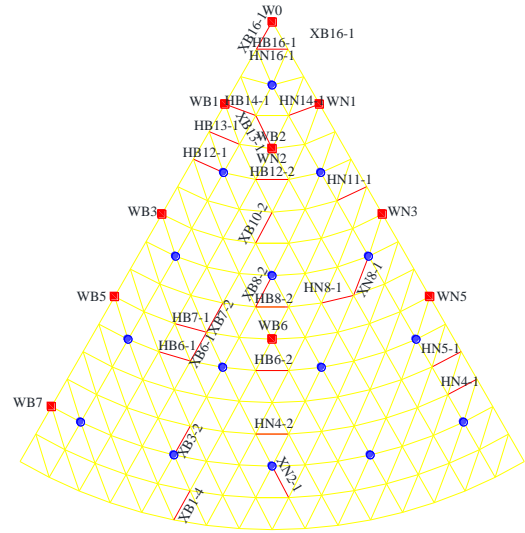

Fig. 10 Arrangement of loading points and measurement points

4.2. Parameter sensitivity analysis

To study the effect of FCCJ on the performance of the global suspen-dome structure, and to calculate the structural response considering the coupling effect of the full-span uniform load and the random variation of FCCJ, the authors extracted the key joint vertical deformations (JVDs), typical member axial stresses (MASs) of the upper reticulated shell, and key radial tension bar internal forces (RBFs), and then their sensitivities to FCCJ were analyzed [33]. To compare JVDs, MASs, and RBFs with the experimental results, a uniform load was simulated as the experimental load and applied to 80 joints as an equivalent concentrated load. The schematic diagram of the loading points is shown in Fig. 10. The blue circles in Fig. 10 indicate the loading points, and a concentrated

load of 1 kN was applied on each point. By considering the symmetry of the structure itself and of the load, the measurement points were concentrated in 1/6th of the area of the K6 reticulated shell, which further simplified the evaluation of PFL [34], and the measurement points are also shown in Fig. 10. By fully considering the stress characteristics of K6, the authors selected two types of measuring members: the ring member (HB) and radial member (XB).

4.2.1. Sensitivity analysis of JVDs to FCs

According to the internal force distribution of the suspen-dome, the lower tensegrity system can play the role of an elastic support for the upper reticulated shell [35], reducing the vertical deformations of the structure under vertical load. Therefore, JVDs are closely related to the pre-stress distribution of the lower tensegrity system, and the friction loss at the cable–strut joint will inevitably affect the vertical deformations of the structure. The graphs of the sensitivity of key JVDs and maximum JVDs to FCCJ are shown in Fig. 11. Owing to space limitation, the graphs show only the most significant results.

As indicated in Fig. 11, all the key JVDs are sensitive to the FCs of the 7th HC, i.e., the outer-most HC, and other FCs near the joint. Specifically, besides the FC of the 7th HC, the JVD w_0 at the mid-span displayed a certain sensitivity to the FC of the 2nd HC near the mid-span, albeit small. The FC at the other cable–strut joints have almost no effect on w_0. The w_4 between the 3rd and 4th HCs is the most sensitive to the FCs μ_{2_1} and μ_{2_2}, followed by the FC of the outer-most HC. It should be noted that the sensitivity of w_4 to the FC of the 2nd HC is stronger than that of the 3rd HC. There are two main reasons for this phenomenon. On the one hand, the pre-stressed design value of the 2nd HC is larger than that of the 3rd HC, causing the strut of the 2nd HC to have a stronger supportive effect on the upper reticulated shell. Therefore, the FC of the 2nd HC had a more profound effect on the mechanical properties of the upper reticulated shell. On the other hand, the radial tension bars at the cable–strut joints corresponding to μ_{2_1} and μ_{2_2} of the 2nd HC are just connected to the area near w_4, and therefore the changes of μ_{2_1} and μ_{2_2} will directly affect w_4. In addition, w_8 between the 6th and 7th HCs is the most sensitive to the FC of the 7th HC near w_8, i.e., μ_{7_33}, μ_{7_34}, μ_{7_35}, μ_{7_36}, μ_{7_37}, μ_{7_42}, followed by the FC of the 6th HC.
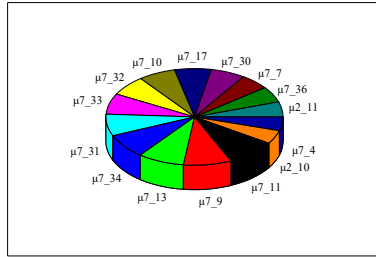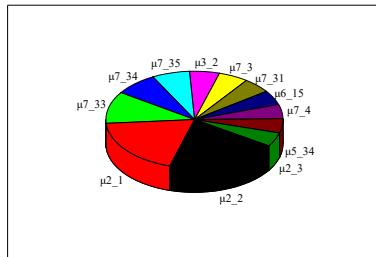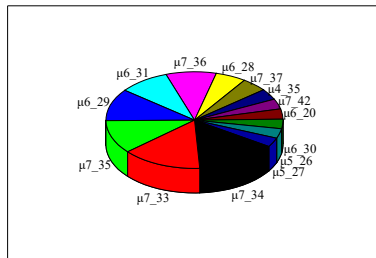
Fig. 12 is a plot of the sensitivity of the maximum JVD w_{max} to the FC. Obviously, w_{max} is mainly sensitive to the FC of the 2nd and 7th HCs. One reason for this is that the pre-stressed value of the outer-most HC is the largest, and the effect on the upper reticulated shell is the most significant. The other reason is that FCs at all cable–strut joints changed to arbitrary values during the calculation process, causing w_{max} to change its position and appear randomly in the area between the 1st and 2nd HCs. The pre-stressed design value of the 2nd HC affecting this area is larger than that of the 1st HC, and therefore w_{max} shows a more significant sensitivity to the FC of the 2nd HC.
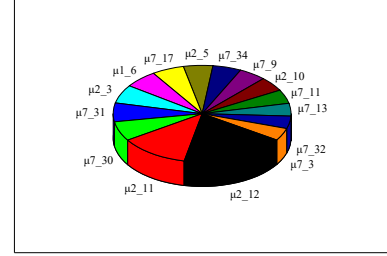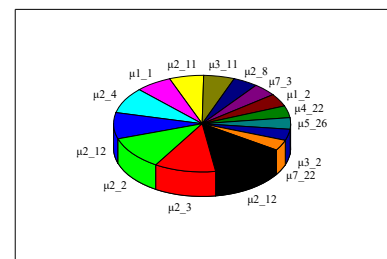

Fig. 12 Sensitivity of maximum JVD w_{max} to the FCs

As shown in Fig. 11, the FC of the outer-most HC has a remarkable effect on the vertical deformations of the entire structure, while those of the other HCs only affect the JVDs near the cable–strut joints. There are two main reasons for this phenomenon. On the one hand, the FC of the outer-most HC affects the design value of its internal force more than that of the other HCs. On the other hand, the outer-most HC is near the edge of the support where all loads born by the reticulated shell are gathered. The outer-most HC plays a decisive role in the structure. Therefore, special attention should be paid to the effect of the FC of the outer-most HC on the suspen-dome structure in the pre-stress construction process.
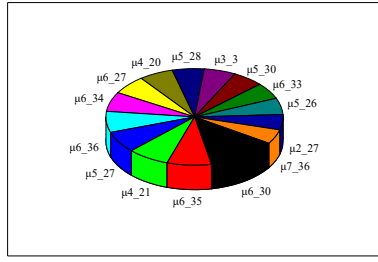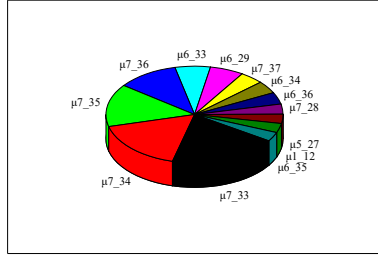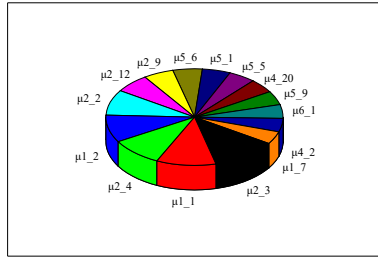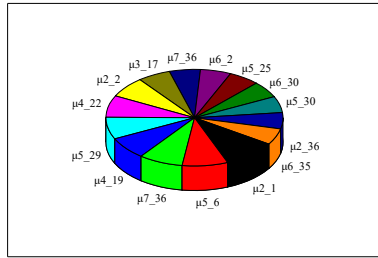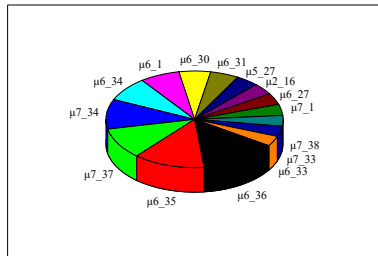
4.2.2. Analysis of sensitivity of MASs to FCs

The purpose of introducing the tensegrity system into the suspen-dome is to improve the mechanical properties of the upper single-layer reticulated shell. Therefore, the changing of FC will inevitably affect the internal force of the lower HC, which in turn will influence the MASs of the upper reticulated shell. To study the effect of FC change on MASs from the inside to the outside of the reticulated shell, HB16-1 and XB16-1 near the mid-span, HB1-1 and XB1-1 near the outermost HC, HB6-1 between the 5th and 6th HCs, XB8-1 between the 4th and 5th HCs were selected. The graphical plots of sensitivity of a typical MAS to the FC were drawn, as shown in Fig. 13.

As indicated in Fig. 13, the radial MAS is as sensitive to the FC as the ring MAS, i.e., the MASs are sensitive to the FC in the adjacent area. The larger the pre-stressed design value in the adjacent area, the more sensitive the MAS. For example, the axial stress of HB6-1, σ_{HB6-1}, is sensitive to μ_{5_j}, and even more so to the FC μ_{6_j} of the 6th HC, with a larger pre-stressed design value. σ_{XB8-1} is sensitive to μ_{4_j} and more sensitive to μ_{5_j} of the 5th HC, with a larger pre-stressed design value. The stresses σ_{HB16-1} and σ_{XB16-1} near the mid-span display remarkable sensitivity to μ_{2_j}, followed by μ_{1_j}. The reason why σ_{HB16-1} and σ_{XB16-1} are less sensitive to μ_{1_j} is that the pre-stressed design value of the 2nd HC is much larger than that of the 1st HC. The stresses σ_{HB1-1} and σ_{XB1-1} show a certain degree of sensitivity to the FCs of the 5th and 6th HCs, and more so to the FC of the 7th HC, which is closer to the area and has a larger pre-stressed design value. As illustrated in Fig. 13, although the JVDs exhibit a more obvious sensitivity to the FC of the outermost HC, most MASs also display a certain degree of sensitivity to the FC of the outermost HC. This also indicates that the effect of FC of the outermost HC on the mechanical properties of the structure needs attention.


a) w_0

b) w_4

c) w_8

Fig. 11 Sensitive of key JVDs to the FCs

a) σ_{HB16-1}

b) σ_{HB6-1}

c) σ_{HB1-1}

d) σ_{XB16-1}

e) σ_{XB8-1}

f) σ_{XB1-1}

Fig. 13 Sensitivity of typical MASs to the FCs

To comprehensively evaluate the effect of FC at all cable–strut joints on the MASs of the upper reticulated shell, a graphical plot of sensitivity of the maximum MAS σ_{wq_max} of the upper reticulated shell to the FC was drawn, as shown in Fig. 14. Fig. 14 reveals that the maximum MAS is most sensitive to the FCs of the 2nd and 3rd HCs. The reason for this might be that when the FC changes

randomly, the stress σ_{wq_max} appears in the area between the 2nd and 3rd HCs, and the FC change will mainly affect the MAS in the adjacent area.
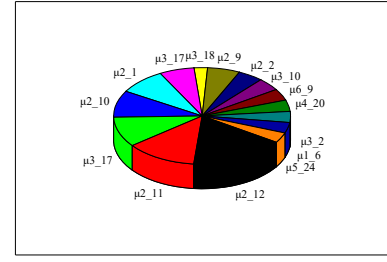
Fig. 14 Sensitivity of maximum MAS σ_{max} to the FCs

The graphs of sensitivity of MAS to FC are similar to those of the JVDs. That is, a change in FC will greatly affect the MASs in the adjacent area but have a smaller effect on the MASs at a position away from the cable–strut joint.

4.3. Effect of random PFL on static structure performance

To investigate the change law of the global structure performance with the change in FCCJ, the probability distribution characteristics of the maximum JVD w_{max}, the maximum MAS σ_{wq_max} and the maximum RBF N_{xls_max} varying randomly with the FCs were obtained [33,36], as shown in Figs. 15–17. The probability distribution index of performance of the suspen-dome is shown in Table 5. Figs. 15–17 show that when the FCCJ of the suspen-dome change arbitrarily, w_{max}, σ_{wq_max}, and N_{xls_max} also vary randomly but follow a broad set of rules. In general, the sample frequency histograms of various mechanical performance indices are low on both sides of graphics, high in the middle, and symmetrical on the left and right sides. The K–S test result shows that the sample data of all mechanical performance indices obey normal distribution in the concentration area, and only a few results are discrete.
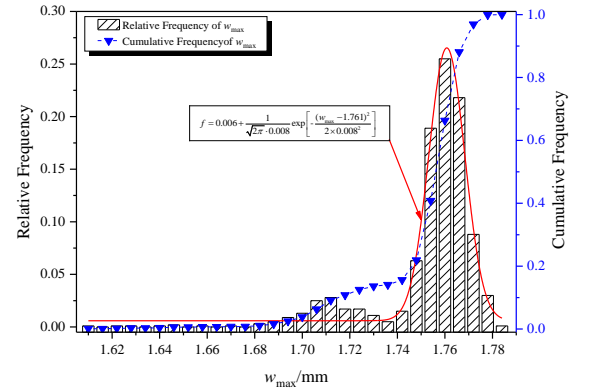
Fig. 15 Probability distribution of w_{max}
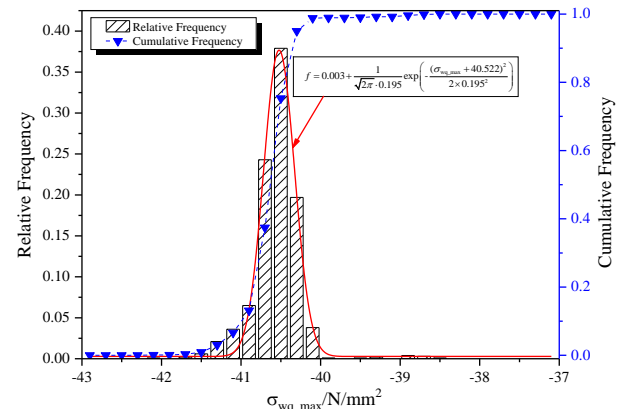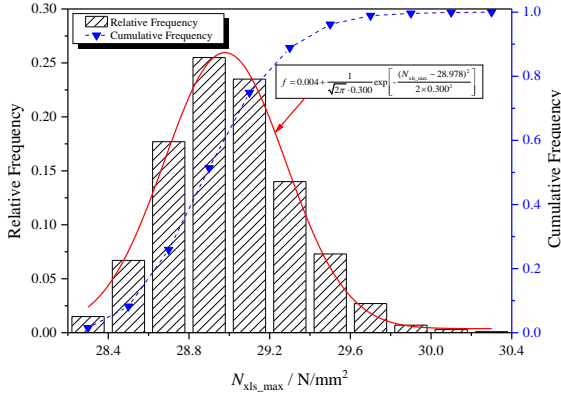

Fig. 16 Probability distribution of σ_{wq_max}

Fig. 17 Probability distribution of N_{xls_max}

Table 5
Probability distribution parameters of various performances

| Item	w_{max} (mm)	σ_{wq_max} (N/mm^2)	N_{xls_max} (N/mm^2)
Mean /μ	1.761	-40.522	28.978
Mean square deviation /σ	0.008	0.195	0.3
Maximum error /R	0.154	1.487	1.021
Percentage increase in maximum error	8.67%	3.67%	4.4%
Exceeding probability (μ-3σ, μ+3σ)	14.20%	1.90%	0.6%

According to the analysis, the structure mainly arches upwards under the action of pre-stress and load, and the maximum JVD is also an upwards arching deformation. The main reason for this is that the global stiffness of the structure is large, and the load applied during the experiment is small. The structural deformation is mainly controlled by the arching effect upon the application of pre-stress. As indicated in Fig. 15, for w_{max}, the mean value μ is 1.761 mm, the mean square deviation σ is 0.008, the maximum value is 1.785 mm, and the minimum value is 1.608 mm. Therefore, the maximum error in the maximum vertical deformation of the upper reticulated shell due to the change of FCCJ, $R_{w\_max} = |1.608-1.761| = 0.153$ mm, and the percentage increase in maximum error is 8.67%. In order to investigate the discrete degree of w_{max}, the exceeding probability (μ-3σ, μ+3σ) should be calculated, i.e., the probability of exceeding (1.738, 1.784) is 14.2%; it can be seen that the discrete degree of w_{max} is small.

To investigate the specific mechanism of the effect of FCCJ on structural deformation, two cases including the absence of friction loss at all cable–strut joints, i.e., $\mu_{i\_j} = 0$, and the FC without random variation with all FCCJs taken as $\mu_{i\_j} = 0.165$ were analyzed. The vertical deformation nephogram was drawn as shown in Figs. 18 and 19. A comparison of Fig. 18 with Fig. 19 reveals that the two cases follow the same deformation distribution laws. That is, under the action of pre-stress and load, the mid-span has the largest upwards arching, and the deformation gradually changes to downwards deflection from inside to outside. However, friction at the cable–strut joint reduces the upwards arching deformation of the structure and adversely affects the structure. When $\mu_{i\_j} = 0$, the maximum upwards arching deformation occurs on the reticulated shell between the 1st and 2nd rings, which is 2.011 mm. When $\mu_{i\_j} = 0.165$, even though it still occurs in the same area, the deformation value reduces to 1.774 mm. By simultaneously comparing this trend with Fig. 15, the authors found that the probability of sample data of the maximum upwards arching deformation considering the RPFL (μ_{i_j} = random) being smaller than that considering μ_{i_j} = 0 is 100%. That is, the friction loss has an inevitable and adverse effect on structural deformation. In addition, if the mean of the sample data is taken as the comprehensive performance index [37], the pre-stressed random friction loss can reduce the upwards arching deformation by (2.011-1.761)/2.011=12.43%. By comparing Fig. 15 with Fig. 19, the authors found that the probability of sample data of the maximum upwards arching deformation considering μ_{i_j} = random being smaller than that considering μ_{i_j} = 0.165 is 96.1%. That is, the actual upwards arching deformation is probably smaller than that considering the FC without random variation. Obviously, if the RPFL is not considered, the effect on the structure will be underestimated.

In summary, although PFL cannot change the deformation distribution law of the entire structure, it will weaken the favorable effect of pre-stress and reduce the upwards arching deformation of the structure under the action of pre-stress and small load. Moreover, it is highly probable that the global upwards arching deformation is smaller when the FC is considered with random variation than without.
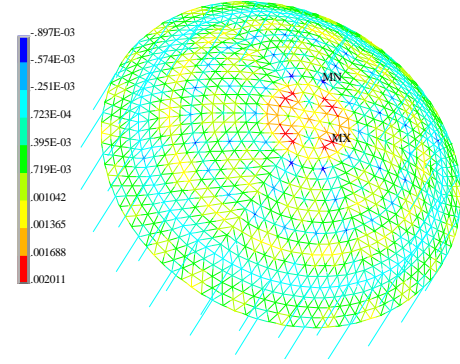
Fig. 18 Vertical deformation nephogram of the upper reticulated shell for $\mu_{i\_j} = 0$ (m)
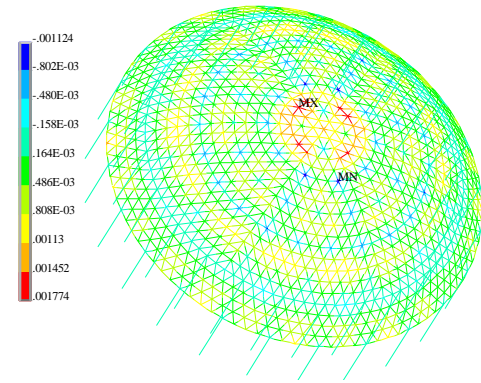
Fig. 19 Vertical deformation nephogram of the upper reticulated shell for $\mu_{i\_j} = 0.165$ (m)

Since the members of the upper reticulated shell are mainly subjected to axial force, and the stress measured by the experiment is axial stress, the maximum MAS σ_{wq_max} was extracted and analyzed. The axial-stress nephograms in the two cases of $\mu_{i\_j} = 0$ and $\mu_{i\_j} = 0.165$ were captured, as shown in Figs. 20 and 21. A comparison of Figs. 20 and 21 reveals that the friction loss does not have a major effect on the stress distribution law of the structure, which is similar with the findings of the structural deformation analysis. In both cases, the stress σ_{wq_max} occurs at the members of the 5th ring of the reticulated shell, and the maximum axial stresses are -42.6 MPa when $\mu_{i\_j} = 0$ and -41.1 MPa when $\mu_{i\_j} = 0.165$, respectively. If the mean value of the sample data in Fig. 16, i.e. -40.522 MPa, were taken as the comprehensive performance index considering the RPFL, the maximum axial stress relative difference of the upper reticulated shell in the three cases would be less than 5%, which can be ignored. This indicates that if or how to consider the friction loss has little effect on the stress σ_{wq_max}.
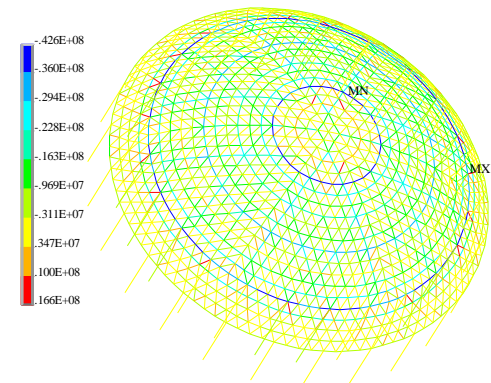
Fig. 20 MAS nephogram of the upper reticulated shell considering $\mu_{i\_j} = 0$ (Pa)
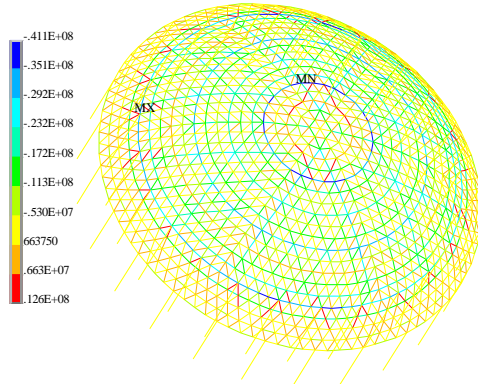
Fig. 21 MAS nephogram of the upper reticulated shell considering $\mu_{i\_j} = 0.165$ (Pa)

The absolute values of the typical MASs of the upper reticulated shell in the three cases were further extracted, and a bar chart was drawn for comparison, as shown in Fig. 22, incorporating PFL or RPFL increases the axial stresses of the upper reticulated shell. For example, when μ_{i_j} = random, the axial stresses of XB13-1 and XB7-2 are increased by 159.24% and 93.83%, respectively. However, by comparing the two ways of considering the friction loss, the authors found that, in most cases, considering μ_{i_j} = random will further increase the axial internal force of the upper reticulated shell. For example, when μ_{i_j} = 0.165, the axial stresses of XB13-1 and HB8-2 are −0.72 and −4.14 MPa, respectively. However, when considering μ_{i_j} = random, the axial stresses are −0.99 and −4.40 MPa, respectively, which are increased by 37.5% and 6.28%, respectively. Therefore, although PFL has little effect on the maximum MAS, it will increase the typical MASs. However, considering the RPFL will greatly increase the member axial stresses, which cannot be ignored.
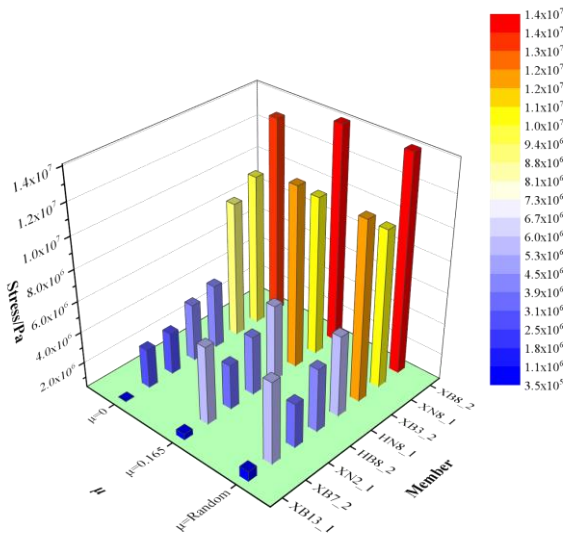

Fig. 22 Bar chart of typical member axial stresses

The RBFs are closely related to the internal forces of the HCs. For the tensegrity system of the structure, the pre-stressing effect should be fully realized to minimize the internal force under the external load. As shown in Table 5, the exceeding probability $(\mu-3\sigma, \mu+3\sigma)$ of the sample data of N_{xls_max} is only 0.6% closer to the normal distribution. The RBF nephograms considering $\mu_{i\_j} = 0$ and $\mu_{i\_j} = 0.165$ were extracted and are illustrated in Figs. 23 and 24, respectively. The distribution law is that the RBFs gradually increase from inside to outside, and the maximum RBFs are 28.2 and 28.9 MPa, respectively. By comparing these results with the random analysis ones in Fig. 17, the probability of sample data greater than 28.2 and 28.9 MPa are 100% and 60%, respectively. Therefore, PFL will increase the RBFs, and RPFL will increase the maximum RBF to a great extent. However, in general, the extent of increase of the maximum RBF is smaller than the maximum JVD.
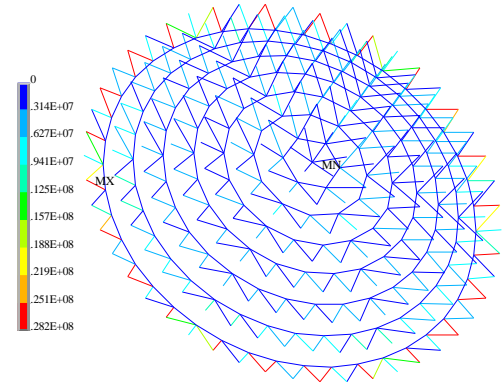

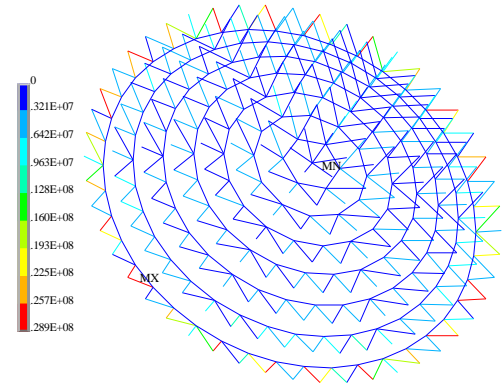**Fig. 23** Radial tension bars internal force nephogram considering $\mu_{i\_j} = 0$ (Pa)

Fig. 24 Radial tension bar internal force nephogram considering $\mu_{i\_j} = 0.165$ (Pa)

4.4. Static loading experiment on scaled-down model

To study the law governing the effect of FCs with random variation on the actual structure's performance, a static loading experiment was carried out after the tension test shown in Fig. 4. During the experiment, a uniform load was applied to 80 joints as the equivalent concentrated load on the upper reticulated shell. The loading points were arranged as shown in Fig. 10. Each loading point was divided into five levels, and a total load of 1 kN was applied. A photograph of the loading experiment is presented in Fig. 25. The representative members and joints of the upper reticulated shell were selected as the stress and deformation measurement points, respectively, and the arrangement of measurement points corresponds to the previous theoretical analysis, as shown in Fig. 11. Since the static loading experiment was an elastic loading experiment, the stresses were obtained by converting the strains measured by a resistance strain gauge attached to the members, and the deformations were obtained by a laser tracker to an accuracy of 0.01 mm [5].

Fig. 25 Photograph of model during loading experiment

To verify the feasibility of the Monte Carlo method to analyse the effect of random friction loss on global structure performance, the experimental results were compared with the finite element calculation results. Firstly, the authors

applied the actual tensioning control force shown in Fig. 7 using a force-finding analysis considering RPFL on ANSYS. Then, the static loading process was simulated according to the experimental loading process, and a random database of structural mechanical responses was generated by the Monte Carlo method. Finally, the random mathematical characteristics were analyzed. Moreover, to clarify the effect of PFL on the structural performance, theoretical values 1 with $\mu_{i\_j} = 0$ and 2 with $\mu_{i\_j} = 0.165$ of the member stresses and joint deformations were calculated. The results of the Monte Carlo calculations of representative member stresses and joint deformations were used to construct a box plot which can reflect the characteristics of the original data distribution. The Monte Carlo calculations were then compared with the experimental values, theoretical values 1 and 2, as shown in Figs. 26–28. As a general trend, the representative member stresses and joint deformations based on μ_{i_j} = random in 1,000 groups were mostly located in the whiskers of the Box plot, in which, the insides of the two whiskers are normal values, while the outsides are outliers. Moreover, the Monte Carlo calculations were basically consistent with the trend of the experimental values, which confirms to a certain extent the feasibility of the probability distribution model of FC μ and Monte Carlo method.

4.4.1. Monte carlo calculations of joint deformation

In Fig. 26, under the action of pre-stress and load, the structural deformation is dominated by upwards arching, and all the deformations of the selected measurement points are positive values. All Monte Carlo calculations of joint deformation of the 11 measurement points selected from the inside to the outside of the reticulated shell obey the normal distribution revealed by the K–S test. Most Monte Carlo calculations are located in the whiskers of the box plot. The general discrete degree of the calculated results is not considerably large. The discrete points of the Monte Carlo calculations at the inner ring of the reticulated shell are close to the lower limit of the normal range. With transition to the outer ring of the reticulated shell, the discrete points become closer to the upper limit of the normal range, such as the change trend of discrete points WN3, WB5, and WB6.
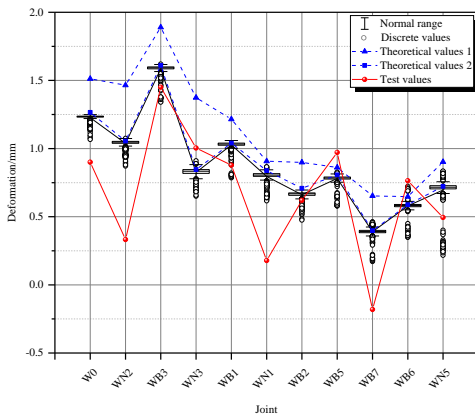

Fig. 26 Distribution contrast diagram of joint deformations

From the comparison of the Monte Carlo calculations, and theoretical values 1 and 2, the authors found that their structural deformation distributions follow the same trend. Both theoretical values 1 and 2 are close to the upper limit of normal range of the Monte Carlo calculations. Most theoretical values 2 are located in the upper whisker of the box plot and are closer to the means. The deformations of all measurement points show that theoretical values 1 are larger than 2 and slightly larger than the Monte Carlo calculations. Obviously, this is because the friction loss was not considered when calculating theoretical values 1, the pre-stressing effect was the largest, and the upper reticulated shell had the largest degree of arching. However, although theoretical values 2 were the deformation responses when all FCs were taken as 0.165, they still slightly deviated from the Monte Carlo calculations, indicating that the relationship between the pre-stress and structural response is non-linear, and the effect of friction loss on the structure performance is also inevitably non-linear.

By comparing the experimental values with the Monte Carlo calculations, the authors found that the structural deformation distribution law reflected by the experimental values was basically consistent with the Monte Carlo calculations, while the experimental values were more discrete. However, the experimental values of WB1, WB2, and WN5 are in the normal range. The experimental values of WB3 and WB6 are in the discrete area, which can be used to verify to a certain extent the feasibility of the random numerical simulation analysis. The experimental values of other measurement points were larger than the Monte

Carlo calculations. The reason might be that the change law of the FCCJ in the experimental model is far more complex than that of the normal distribution model in the calculated model.

As indicated in Fig. 6, μ varies non-linearly with the tension, but it does not always maintain the mean value of 0.165. When the pre-stress is less than 10 kN, μ is more discrete. When the pre-stressed design value is approximately 5 kN, μ is approximately 0.22, and the tension of the six HCs in the inner structure are less than 5.04 kN, the FC will be greater than the mean, but the tension of the outermost HC is 11.5 kN, whose FC is closer to the mean of 0.165, and it will agree with the normal distribution random mathematical model of FC.

In Section 4.2, the PFL of each HC mainly affects the deformation of the reticulated shell in the adjacent area. In the experimental model, the upwards arching deformation of the inner HC under the action of pre-stress and light load is small than that of the outer HC, because the actual friction loss of the inner HC is larger. This implies that most of the experimental values of the HCs are close to the lower limit of normal range of the Monte Carlo calculations, but the experimental values of the inner HC are farther away from the lower limit of the normal range than that of the outer HC.

4.4.2. Monte carlo calculations of radial member stress

Five representative radial members were selected, and the member stresses were extracted. A distribution contrast diagram of Monte Carlo calculations, theoretical values 1, theoretical values 2 and experimental values was drawn, as shown in Fig. 27. It shows that the representative radial member stresses of the upper reticulated shell based on 1,000 groups of random values of μ_{i_j} through the K–S test display an approximate optimal normal distribution, which is more conducive to data analysis. Only a few values of the members are beyond the normal range, albeit without large discreteness. In general, because of the small experimental load, the representative radial member stresses are small, and the Monte Carlo calculations were basically consistent with the distribution law of experimental values, which verifies the correctness of the theoretical analysis.

The calculated value of the inner-most radial member, XB16-1, deviates remarkably from the experimental value, when compared with the other representative members. The main reason for this phenomenon is that the pre-stressed design value of the inner HC is small, and the corresponding FCs are extremely unstable, causing the stresses in the corresponding area of the reticulated shell to fluctuate. This is consistent with the fact that the experimental values of the representative joint deformation near the mid-span deviates from the calculated values as shown in section 4.4.1. In addition, the comparison of theoretical values 1 and 2 and the Monte Carlo calculations showed that both theoretical values 1 and 2 were close to the upper limit of the normal range, while theoretical value 2 was basically distributed within the normal range. However, theoretical value 2 deviates from the mean of the Monte Carlo calculations; the reason being similar to that for the joint deformations. The means of the Monte Carlo calculations were slightly greater than theoretical values 1 and 2 and were closer to the experimental values. Moreover, considering that the selected radial members were all under pressure, the calculated result considering RPFL was more conservative, and therefore more suitable for the actual situation.
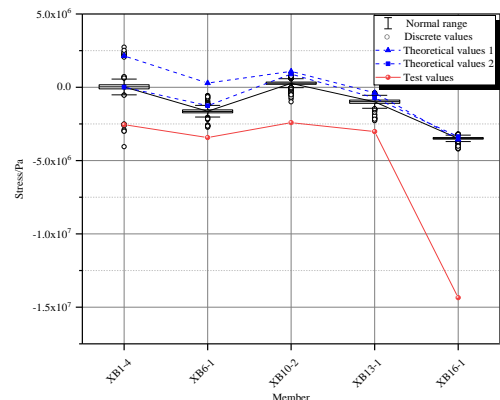
Fig. 27 Distribution contrast diagram of radial member stresses

4.4.3. Monte carlo calculations of ring member stress

Fourteen representative ring members were selected, and the member stresses were extracted, and the corresponding distribution contrast diagram is shown in Fig. 28. According to the box plot of the Monte Carlo calculations, the ring member stresses change from the tension at the supports to the compression near the mid-span of the reticulated shell. Tensioned ring members appeared at the mid-span with small absolute values. There were few differences between the Monte Carlo calculations of the ring members at the same ring, such as HN4-

1 and HB4-2, HB6-1 and HB6-2, HB12-1 and HB12-2, HB14-1 and HN14-1, HB16-1 and HN16-1, and so were the experimental values. The trend of experimental values was almost the same as those of the Monte Carlo calculations, and the two values did not differ much. This indicates that the experimental design and process met the requirements, and the probability distribution model of FC μ and the Monte Carlo method are feasible within a certain extent. Here, the authors emphasize that the calculated values of the inner-most HCs, HB16-1 and HN16-1, deviate significantly from the experimental values. The reason for this is the same as that of the representative joint deformations and radial member stresses near the mid-span. The comparison of the Monte Carlo calculations with theoretical values 1 and 2 showed that theoretical value 1 was almost entirely within the normal range of the box plot. This in turn indicates that the ring member stresses in the two cases with $\mu_{i\_j} = 0$ and $\mu_{i\_j} = 0.165$, respectively, are not considerably different. As displayed in Figs. 27–28, the Monte Carlo calculations are more volatile than theoretical value 1, indicating that PFL would make the internal force distribution of the structure uneven.

In general, the absolute values of calculated results, such as the joint deformations and radial and ring member stresses, considering RPFL and based on the Monte Carlo method are smaller than the experimental values. This occurred because of the exposure of the experimental model to corrosion outdoors for one year. In addition, installation errors may have exaggerated the experimental values. The smaller value shows that, in an actual suspen-dome structure, there are factors besides FCCJ which may cause additional pre-stressed losses. This fact cannot be ignored in engineering practice. Initial defects such as the initial eccentricity, member initial curvature and RPFL will be considered throughout Section 5, along with an analysis of the effect of coupling on the ultimate bearing capacity of the suspen-dome.
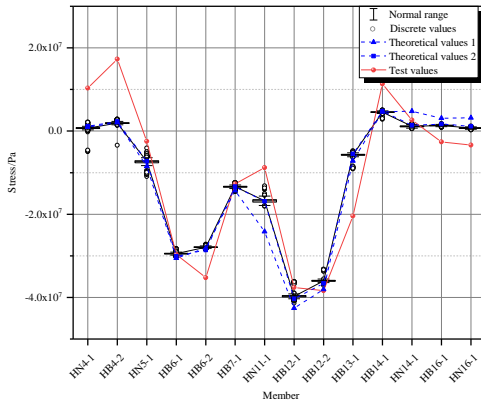

Fig. 28 Distribution contrast diagram of ring member stresses

5. Analysis of effect of multi-defect random variation coupling on ultimate bearing capacity of suspen-dome structure

According to the analysis in Section 4.4, the experimental values are slightly different from the calculated values. The reasons cited included the possible deviation of FCCJ in the theoretical calculation model from that in the actual experimental model. In addition, there inevitably exist initial defects, such as the member initial curvature, installation and positioning deviations, and section-size deviation of members in the experimental model during manufacturing and installation. Among them, the section size of members is small and the slenderness ratio is large in the scaled-down model, causing initial curvature during the process of transportation and installation. The upper reticulated shell is a defect-sensitive structure [38]. Therefore, the effect of joint installation deviation on the structure performance cannot be ignored. To obtain the actual performance of the structure and establish a theoretical model which can characterize the true operational performance of the structure, this paper introduces the member initial curvature and joint installation deviations based on RPFL, to evaluate the actual structure performance.

5.1. Initial curvature and installation deviation

Initial curvature is inevitable during the processes of manufacturing, transportation, and installation of members, causing members to produce a P–Δ effect under an axial force. The initial curvature strongly influences the structure's mechanical properties [39]. The shape of the member during the initial curvature is random. For ease of calculation and structural safety, the *sine* half-wave curve was used to simulate the initial curvature, as shown in Fig. 29. The multi-segment beam method was used to simulate the initial curvature defect

[40]. That is, after the ideal straight rod element was subdivided into multi-segment beam elements with a rigid connection, the coordinates of the intermediate connection nodes were adjusted by a *sine* half-wave curve. To ensure accurate analysis, this paper assumes the number of segments as 10.
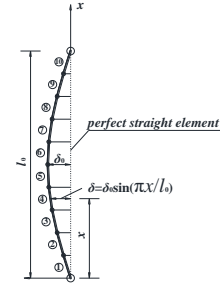

Fig. 29 Schematic diagram of initial curvature defect of member

After determining the initial curvature form of the member, the authors found that the key parameter affecting the initial curvature defect degree was the bending amplitude δ_0 in the mid-span. Apparently, δ_0 of each member changes randomly. However, to ensure structural safety, the literature [41] has set a limit on the axial bending height of the space grid structure member, i.e., $\delta_0 \leq l_0 / 1,000$, where l_0 is the original length of the member. Combined with the actual on-site installation conditions and the size effect of the scaled-down model, the δ_0 of the experimental model was appropriately enlarged to $\delta_0 = l_0 / 600$. Because there are few published material on the random parameters of a member's initial curvature, this paper refers to the literature [41] and assumes that the random variable δ_0 obeys the extreme value I-type distribution. Its probability density function $f(\delta_0)$ is as follows.

$$f(\delta_0) = \frac{1}{\sigma} \cdot e^{\frac{\delta_0 - \mu}{\sigma}} \cdot e^{-e^{\frac{\delta_0 - \mu}{\sigma}}} \tag{5}$$

Assuming that the exceeding probability of bending amplitude $\delta_0 = l_0 / 600$ is 2.5%, and the exceeding probability of $\hat{\delta}_0 = 0$ is 1%, the mean μ and mean square deviation σ of δ_0 of each member were calculated as follows.

$$\mu = 0.78(\frac{l_0}{600}) \approx \frac{l_0}{770} \tag{6}$$

$$\sigma = \frac{l_0/600}{5.9} = \frac{l_0}{3540} \tag{7}$$

The upper reticulated shell had a total of 3,504 members. The Monte Carlo method was used to analyze the effect of random variation of the member initial curvature on the structural ultimate bearing capacity. Assuming that the ultimate bearing capacity's sample library was formed by iteratively and randomly running the calculations n times, for each random simulation, a group of initial curvature amplitude random-sample library $\{\boldsymbol{\delta}_0\}=(\delta_{1,j}, \delta_{2,j}, \delta_{3,j}, \ldots \delta_{i,j}, \ldots \delta_{3504,j})$ was generated, where i is the member number and j is the *No. j* random simulation iterative calculation. Moreover, $\delta_{i,j}$ is independent and obeys the extreme value I-type distribution. Fig. 30 shows the FEM of the random simulation process.
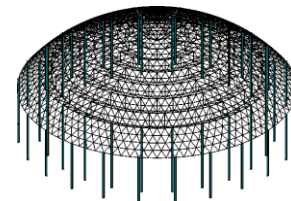

Fig. 30 Model diagram of member initial curvature ($\times 10$)

5.2. Analysis of effect of multi-defect random variation coupling on ultimate bearing capacity

To accurately evaluate the ultimate bearing capacity of the structure, an

FEM of the experimental model was constructed, and defects such as the member initial curvature random defect, RPFL, and installation deviation were introduced. The member initial curvature amplitude δ_0 and the FC μ_{i_j} at each cable–strut joint are random, independent variables. In general, to analyze the ultimate bearing capacity considering the double non-linearity of the material and the geometry is analyzed, the arc-length method is used. However, given that the calculation is not easy to converge, and the cost is relatively high, the authors assumed that when the calculation does not converge in the analysis process, i.e., the stiffness matrix of the structure appears singular, the structure has lost its stability. Meanwhile, the load corresponding to the load step can be considered as the structural ultimate bearing capacity.

Fig. 31 illustrates a probability distribution curve of the ultimate bearing capacity, which tended to converge when the simulation time was 100. The sample data distribution is similar with the normal distribution, except that it moves to the right and forms a peak in the interval (4.5, 5.0). The results at the tail are called *stragglers*. Furthermore, most of the relative frequency curve of the sample data is located in the 95% confidence interval of the fitted LogNormal curve. Therefore, P_{cr} obeys the LogNormal distribution with the parameter (ln(4.62),0.19), and the maximum and minimum values are 5.454 and 2.965 kN, respectively.
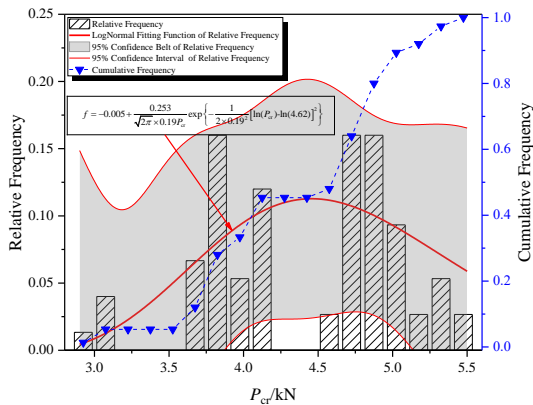

Fig. 31 Probability distribution diagram of ultimate bearing capacity

To further analyze the effect of initial defects on the ultimate bearing capacity of the suspen-dome, the ultimate bearing capacity under two conditions, without friction loss, i.e., ideal structure with $\mu_{i\_j}=0$, and with the same friction loss at all cable–strut joints, i.e., defining all $\mu_{i\_j}=0.165$, were calculated. The results were compared with those considering the friction loss, member initial curvature, and joint installation deviation simultaneously, which can be seen in Table 6. The ultimate bearing capacity with $\mu_{i\_j}=0$, which is 9.05 kN is larger than that with $\mu_{i\_j}=0.165$, which is 5.49 kN. The ultimate bearing capacity with the same friction loss at all cable–strut joints is reduced by 39.34%, when compared with that of an ideal structure. Then, the axial stress and deformation nephograms of the upper reticulated shell were extracted to analyze the specific effect of friction loss on the structure's performance. As shown in Table 6, when structural failure occurs, the inner members are mainly subjected to compression, while the outer members are subjected to tension. However, the ideal structure has a uniform stress distribution at failure, and the maximum compressive stress appears in the area to which the concentrated load was applied. Further, the stress level of the ideal structure is significantly higher than that of the structure with friction loss at structural failure occurs. Obviously, this is because the stress distribution of the ideal structure is uniform and the structural stiffness is large, thus allowing the structure to bear larger loads. Therefore, its stress level is significantly improved, which greatly improves the structure's performance.

A comparison of the deformation nephograms of the upper reticulated shell reveals that the maximum deformation of the ideal structure reaches 60.998 mm, which occurs in the area in which the maximum axial stress is generated. Moreover, it is much larger than the maximum deformation of 14.214 mm, considering the friction loss. In addition, deformation in the ideal structure is mainly concentrated in the load-bearing mid-span. After the introduction of friction loss, the deformation range of the structure was expanded, which illustrates the adverse effect of PFL on structural stiffness.

The model state is the closest to the actual state of the structure when simultaneously considering multiple random defects. Meanwhile, the ultimate bearing capacity sample data of 100 groups were all less than 9.05 and 5.49 kN, indicating that the ultimate bearing capacity of the suspen-dome reduces when incorporating multi-defect random variation coupling. If the mean of bearing capacity is taken as a comprehensive performance index of the structure, the bearing capacities reduce by 51.16% compared with the ideal structure and 19.49%

compared with the structure with the same FCCJ. If the friction loss at the cable–strut joint is neglected, the safety of the suspen-dome structure will be seriously overestimated. Likewise, the structural bearing capacity will also be overestimated without considering the random characteristics of each defect.

Table 6
Comparison of structure performance in three cases

Items	Ultimate bearing capacity (kN)	Axial stress nephogram at structural failure (Pa)	Deformation nephogram at structure failure (m)
$\mu_{i\_j}=0$	9.05		
$\mu_{i\_j}=0.165$	5.49		
Multiple random defects	mean	mean square deviation	
	4.42	0.6201	

6. Conclusions

The high efficiency of the suspen-dome structure lies in the accurate introduction of pre-stress. However, due to the inevitable friction loss at cable–strut joints during the construction process, the structure's mechanical properties are affected. Based on the random characteristics of FCCJs, the random analysis of structural mechanical performance of a suspen-dome 1:10 scaled-down experiment model was carried out in this paper. The main conclusions are as follows:

1) Based on the static force balanced relationship and the friction transmission law, a cable force calculation method considering the unequal tension at both sides and the independent change of the FCCJs was proposed, and the reliability of this method was verified by comparing and analyzing the distribution law and relative error of the calculated values and the test values.

2) Engineering and experimental investigations have found that the FCCJs have a large variability, and the investigation data of the rolling cable–strut joint showed that the FCCJs used in the model approximately follows a normal distribution. The mean value is 0.165, and the mean square deviation is 2.665.

3) Random finite element analysis considering the random friction loss of the suspen-dome structure found that when the FCs at all cable–strut joints change randomly, the maximum deformation of the structure will approximately obey the normal distribution. The probability of the random calculation result of the pre-arching deformation value of the structure being less than the deterministic calculation result is as high as 96.1%, a high probability event. The MASs and the RBFs are sensitive to the FCCJs in the adjacent area. Although the maximum MAS of the upper reticulated shell and the maximum RBF follow the normal distribution, compared with the pre-stressed friction loss deterministic analysis results, the random friction loss of the pre-stress will further increase the MASs of the upper reticulated shell and the RBFs. This makes the internal force distribution of the structure uneven. Overall, the effect of random friction loss on the internal force of the structure is less than its effect on deformation. The static loading experiment results of the structure showed that most of the experimental values of key member stress and key joint deformations are within the normal range of the Monte Carlo random simulation calculation results. The changing trend of the calculated values and the experimental values are the same, verifying the feasibility of the Monte Carlo simulation.

4) When simultaneously considering friction loss, member initial curvature, and joint installation deviation, the ultimate bearing capacity with the random variation of each defect of the suspen-dome is reduced by 51.16% compared with the ideal structure and 19.49% compared with the structure with the same friction coefficient at cable–strut joints.

5) In this study, the effect of random pre-stressed friction loss on structural performance was investigated for a specific suspen-dome scaled-down experiment model. The probability distribution model of the FC is obtained from a cable-joint tension test, which was carried out by our research group earlier,

but the amount of the test data is relatively small. In the meantime, owing to the size effect, the random mathematical model of joint friction coefficients in the scaled-down model may differ from the actual project. In the next step, the group will investigate and establish a sample library of slip FCs of various types of cable-support joints in real projects and establish a more accurate probability distribution model of FCs to verify the influence law of random friction losses on actual engineering structures.

Acknowledgments

References

[1] J. G. Cai, Y. Q. Liu, J. Feng, et al., "Nonlinear stability analysis of a radially retractable suspen-dome", *Advanced Steel Construction*, Vol. 13, No. 2, pp. 117-131, 2017.

[2] M. Kawaguchi, M. Abe, and T. Ikuo, "Design, tests and realization of 'suspend-dome' system", *Journal of the International Association for Shell and Spatial Structures*, Vol. 40, No. 3, pp. 179-192, 1999.

[3] H. N. Li, C. L. Yuan, L. Ren et al., "Structural health-monitoring system for roof structure of the Dalian Gymnasium", *Advances in Structural Engineering*, Vol. 22, No. 7, pp. 1579-1590, 2019.

[4] Z. H. Chen, "Cable-supported Structure system", *Science Press*, Beijing, China, 2013.

[5] Z. H. Chen, R. Z. Yan, X. D. Wang et al., "Experimental researches of a suspen-dome structure with rolling cable-ctrut joints", *Advanced Steel Construction*, Vol. 11, No. 1, pp. 15-38, 2015.

[6] R. Montuori and R. E. Skelton, "Globally stable tensegrity compressive structures for arbitrary complexity", *Composite Structures*, Vol. 179, pp. 682-694, 2017.

[7] S. D. Guest, "The stiffness of tensegrity structures", *IMA Journal of Applied Mathematics*, Vol. 76, No. 1, pp. 57-66, 2010.

[8] A. L. Zhang, X. C. Liu, D. M. Wang et al., "Static experimental study on the model of the suspend-dome of the Badminton Gymnasium for 2008 Olympic Games", *Journal of Building Structures*, Vol. 28, No. 6, pp. 58-67, 2007.

[9] G. F. Zhang, S. L. Dong, X. Zhuo et al., "Experimental research on sliding cable prestress losses of suspen-dome structures", *Spatial Structures*, Vol. 26, No. 4, pp. 36-41, 2020.

[10] H. B. Liu and Z. H. Chen, "Structural behavior of the suspen-dome structures and the cable dome structures with sliding cable joints", *Structural Engineering and Mechanics*, Vol. 43, No. 1, pp. 53-70, 2012.

[11] H. B. Liu, Q. H. Han, Z. H. Chen et al., "Precision control method for the pre-stressing construction of suspen-dome structures", *Advanced Steel Construction*, Vol. 10, No. 4, pp. 404-425, 2014.

[12] Z. W. Zhao, B. Liang, R. Z. Yan et al., "A novel numerical method for considering friction during pre-stressing construction of cable-supported structures", *International Journal of Steel Structures*, Vol. 18, No. 5, pp. 1699-1709, 2018.

[13] Y. Chen, Q. Sun, and J. Feng, "Improved form-finding of tensegrity structures using blocks of symmetry-adapted force density matrix", *Journal of Structural Engineering*, Vol. 144, No. 10, pp. 04018174.1-04018174.13, 2018.

[14] J. Y. Zhang and M. Ohsaki, "Force identification of prestressed pin-jointed structures", *Computers & Structures*, Vol. 89, No. 23, pp. 2361-2368, 2011.

[15] M. Ohsaki and J. Y. Zhang, "Nonlinear programming approach to form-finding and folding analysis of tensegrity structures using fictitious material properties", *International Journal of Solids and Structures*, Vol. 69-70, pp. 1-10, 2015.

[16] H. J. Liu, L. F. Yang, Y. L. Li et al., "Geometrically nonlinear analysis on a double controlled form finding method considering construction process of suspen-domes", *Advanced Materials Research*, Vol. 904, pp. 524-527, 2014.

[17] J. M. Guo and D. Zhou, "Pretension simulation and experiment of a negative Gaussian curvature cable dome", *Engineering Structures*, Vol. 127, pp. 737-747, 2016.

[18] Y. Chen, P. Sareh, J. Feng et al., "A computational method for automated detection of engineering structures with cyclic symmetries", *Computers & Structures*, Vol. 191, pp. 153-164, 2017.

[19] Y. Chen, J. Feng, and Q. Sun, "Lower-order symmetric mechanism modes and bifurcation behavior of deployable bar structures with cyclic symmetry", *International Journal of Solids and Structures*, Vol. 139, pp. 1-14, 2018.

[20] Y. Chen, J. Feng, R. Ma et al., "Efficient symmetry method for calculating integral prestress modes of statically indeterminate cable-strut structures", *Journal of Structural Engineering*, Vol. 141, No. 10, pp. 04014240.1-04014240.11, 2014.

[21] Y. Chen, J. Feng, H. Lv et al., "Symmetry representations and elastic redundancy for members of tensegrity structures", *Composite Structures*, Vol. 203, pp. 672-680, 2018.

[22] M. Elhoseny, A. Tharwat, A. E. Hassanien et al., "Bezier curve based path planning in a dynamic field using modified genetic algorithm", *Journal of Computational Science*, Vol. 8, No. 4, pp. 1-41, 2017.

[23] S. Z. Weng and P. Huang, "Principles of Tribology", T*singhua University Press*, Beijing, China, 2002.

[24] S. V. Shil'ko, D. A. Chernous, T. V. Ryabchenko et al., "Estimation of the friction coefficient of a nanostructured composite coating", *Mechanics of Composite Materials*, Vol. 53, No. 5, pp. 579-588, 2017.

[25] D. Prayogo and Y. T. T. Susanto, "Optimizing the prediction accuracy of friction capacity of driven piles in cohesive soil using a novel self-tuning least squares support vector machine", *Advances in Civil Engineering*, Vol. 2018, 6490169.1-6490169.9, 2018.

[26] Y. Chen, J. Feng, P. Sheng et al., "Anti-sliding performance of cable clips of inner concave cable arches in the New Guangzhou Railway Station", *Journal of Building Structures*, Vol. 34, No. 5, pp. 27-32, 2013.

[27] S. Wang, G. J. Zhang, A. L. Zhang et al., "The prestress loss analysis of cable-strut Joint of the Badminton Gymnasium for 2008 Olympic Game", *Journal of Building Structures*, Vol. 28, No. 6, pp. 39-44, 2007.

[28] J. Qin, Z. Q. Wang, R. Zhang et al., "Study on prestress construction monitoring of Badminton Gymnasium for 2008 Olympic Games", *Journal of Building Structures*, Vol. 28, No. 6, pp. 83-91, 2007.

[29] X. C. Liu, A. L. Zhang, and W. L. Fu, "Cable tension preslack method construction simulation

[30] Z. X. Guo, Y. Q. Wang, B. Luo et al., "Prestressed cable construction of large-span suspend-dome in Ji'nan Olympic Center Gymnasium", *Construction Technology*, Vol. 37, No. 5, pp. 133-135, 2008.

[31] Y. B. Yuan, X. Z. Hu, X. D. Cai et al., "Test study on the stress of cable-clamp joint in Xuzhou Olympic Gymnasium", *Low Temperature Building Technology*, Vol. 35, No. 8, pp. 81-83, 2013.

[32] Z. H. Chen, X. X. Wang, H. B. Liu, et al., "Failure test of a suspendome due to cable rupture", *Advanced Steel Construction*, Vol. 15, No. 1, pp 23-29, 2019.

[33] R. Z. Yan, Z. H. Chen, X. D. Wang et al., "Analysis of static performances of suspen-dome structures considering the random errors influence of prestressing construction", *Spatial Structures*, Vol. 21, No. 1, pp. 39-89, 2015.

[34] Y. Chen, J. Feng, and R. J. Ma, "A unified criterion for movability of kinematically indeterminate frameworks with symmetry", *Journal of Building Structures*, Vol. 36, No. 6, pp. 101-116, 2015.

[35] Z. H. Chen, "Suspen-dome Structure", *Science Press*, Beijing, China, 2010.

[36] A. Petcherdchoo, "Probability-based sensitivity of service life of chloride-attacked concrete structures with multiple cover concrete repairs", *Advances in Civil Engineering*, Vol. 2018, 4525646.1-4525646.17, 2018.

[37] G. C. Wu, "Probability and Mathematical Statistics", *China Renmin University Press*, Beijing, China, 2011.

[38] M. Zhang, Y. P. Liu, Z. X. Yu, et al. "Study of seismic resistance of Kiewit-8 dome considering key structural design parameters", *Advanced Steel Construction*, Vol., 15, No. 4, pp. 386-397, 2019.

[39] Y. Ding, T. L. Zhang, "Research on influence of member initial curvature on stability of single-layer spherical reticulated domes", *Advanced Steel Construction*, Vol. 15, No. 1, pp. 9-15, 2019.

[40] J. C. Yan, F. Fan, and Z. G. Cao, "Research on influence of initial curvature of members on elasto-plastic stability of reticulated shells", *Journal of Building Structures*, Vol. 33, No. 12, pp. 63-71, 2012.

[41] Ministry of Housing and Urban-Rural Development of the People's Republic of China, "JGJ 7-2010 Technical Specification for Space Frame Structures", *Architecture & Building Press*, Beijing, China, 2010.